Observation of strong relativistic and distorted-wave effects in $(e, 2e)$ electron-momentum spectroscopy of mercury

Shenyue Xu,[1] Chao Ma,[1,2] Enliang Wang,[2] Pengfei Hu,[1] Xing Wang,[1] Yongtao Zhao,[1] Zhongfeng Xu,[1] Jingkang Deng,[3] Chuangang Ning,[3] Alexander Dorn,[2] and Xueguang Ren[1,2,*]

[1]*School of Science, Xi'an Jiaotong University, Xi'an 710049, China*

[2]*Max-Planck-Institut für Kernphysik, 69117 Heidelberg, Germany*

[3]*Department of Physics, State Key Laboratory of Low-Dimensional Quantum Physics, Tsinghua University, Beijing 100084, China*

(Received 25 October 2018; published 15 February 2019)

We report a measurement of the valence orbital-momentum profiles of mercury (Hg) using a high-sensitivity binary $(e, 2e)$ electron-momentum spectrometer at incident energies of 600 and 1200 eV plus the binding energy. The $6s_{1/2}$ orbital and the spin-orbit components of $5d_{5/2}$ and $5d_{3/2}$ orbitals are well separated in the measured binding-energy spectra. The experimental momentum distributions for the individual orbitals and the branching ratio of $5d_{5/2}$ to $5d_{3/2}$ are obtained and compared with predictions from a plane-wave impulse approximation (PWIA) in which the orbital wave functions are calculated using the nonrelativistic (NR) and spin-orbital (SO) relativistic theories. The SO relativistic calculations are in better agreement with experiment than the NR, indicating clearly the importance of relativistic effects in the electronic structure of Hg. We also observe some discrepancies between experiment and PWIA calculations in the high-momentum region of $6s_{1/2}$ and the low-momentum region of $5d$ orbitals which display a dynamic dependence on the impact energy. These discrepancies become smaller at a higher energy of about 1200 eV and thus can be qualitatively assigned to the distorted-wave effect in the $(e, 2e)$ reaction of Hg.

DOI: 10.1103/PhysRevA.99.022705

I. INTRODUCTION

It has been recognized since the early 1970's [1–4] that many aspects of the physical and chemical properties of heavy atoms and their compounds are determined by the influence of relativistic effects on their electronic structure. Recent calculations have consequently shown the influence of relativity on the color and bond lengths of heavy-metal chemical compounds, as well as its importance in catalysis. This can explain, for example, the color of gold carbene complexes [5] and the low melting point of mercury [6]. The phenomena observed in compounds of heavy atoms such as phosphorescence, magnetism, or the tendency for high valency in chemical reactions can be traced back to relativistic effects determining their electronic structure [1–6].

Electron-momentum spectroscopy (EMS) or binary $(e, 2e)$ spectroscopy is a powerful tool for studying the electronic structure of atoms, molecules, and solids [7–11]. It is based on a kinematically complete electron-impact ionization or $(e, 2e)$ experiment near the so-called Bethe ridge condition. Within the plane-wave impulse approximation (PWIA), the $(e, 2e)$ cross section measured with high-energy electrons ($\sim$1000eV) can be directly related to the electron density distribution in momentum space for the ionized orbital. This is the orbital electron-momentum profile defined as the square modulus of its wave function in momentum space [8,9]. As a result, the measured cross sections usually do not depend on the impact energy [7–11]. This technique allows one to measure both the binding energy and the electron-momentum distribution for each individual orbital. With respect to this, EMS can be regarded as a sensitive probe of how relativistic effects in heavy-element contained systems influence the energies of the different electronic spin orbitals and also the orbital electronic structure.

The first seminal works of relativistic effects in heavy atoms using the EMS method were reported by Mitroy and Fuss [12] and Cook *et al.* [13] in the 1980's. Since then, several EMS measurements in heavy-element atoms and their compounds have been performed (see, e.g., Refs. [14–23]). Among these studies, theory has predicted the strong relativistic effect in the electron-momentum distributions of the $6s$ and $5d$ orbitals of mercury [12].

In the present work, we conducted high-resolution and high-sensitivity EMS experiments for the valence orbitals of mercury (Hg) at projectile energies of about 600 and 1200 eV in order to trace the relativistic effects in its electronic structures and also to examine the possible distorted-wave effects in EMS as a function of impact energy [24–30]. The binding-energy spectra which cover the binding energies ranging from 5 to 20 eV were measured with high statistical accuracy. The spin-orbital relativistic effects of Hg were clearly observed by the measurements of the momentum distributions for the individual orbitals of $6s_{1/2}$, $5d_{5/2}$, and $5d_{3/2}$ and the cross-section ratio of $5d_{5/2}$ to $5d_{3/2}$ as a function of the momentum which were compared with the nonrelativistic and spin-orbital relativistic calculations using density functional theory [31,32].

This paper is organized as follows. After a brief description of the experimental apparatus in Sec. II, we summarize the

*renxueguang@xjtu.edu.cn

essential points of the theoretical calculations in Sec. III. The results are presented and discussed in Sec. IV, before we finish with the conclusions in Sec. V.

II. EXPERIMENTAL SETUP

The experiment was performed using a high-resolution and high-sensitivity $(e, 2e)$ electron-momentum spectrometer. The details of this apparatus have been reported in previous works [33–36] and hence will not be repeated here. Briefly, a double toroidal energy analyzer is equipped with two position- and time-sensitive detectors to detect the two outgoing electrons in coincidence. It utilizes a noncoplanar symmetric geometry, i.e., the two outgoing electrons have almost equal energies and equal polar angles ($\theta_a \approx \theta_b = 45^\circ$) with respect to the direction of the incident electron beam. By using position-sensitive electron detectors the measurement can be done for a range of electron energies and azimuthal scattering angles simultaneously. Therefore, the data-acquisition efficiency is greatly increased with respect to conventional single energy and angle detection techniques. The electron beam was produced by an electron gun equipped with an oxide cathode, which can work at a much lower temperature (∼1100 K), and thus a lower-energy spread of about 0.3 eV of the electron beam can be achieved.

In the present experiment, the low vapor density of Hg and the low $(e, 2e)$ cross sections especially for the $5d$ ionization channel, as well as its known toxicity have posed a major challenge for the EMS measurements of Hg. Here, the gas line outside and inside the vacuum chamber was gradually heated up to ∼100 °C to maintain a stable and high-density Hg gas target in the $(e, 2e)$ reaction zone. Moreover, the pass energy of the toroidal analyzer was set to 100 eV instead of the commonly used 50 eV to increase the detection efficiency of the electrons. It took about 2 months of data collection time in order to obtain a sufficiently high statistic accuracy of the experimental data, especially for the $5d$ ionization channel. The binding-energy resolution in the present work is about 1.1 eV, and angular resolutions are $\Delta\theta = \pm 0.6^\circ$, and $\Delta\phi = \pm 0.85^\circ$, respectively, which were obtained with a calibration measurement on argon.

Using energy and momentum conservation, the binding energy ε and recoil ion momentum $\vec{q}$ can be determined with the measurements of energies and momenta of the incident electron (E_0 and $\vec{p}_0$) and the two outgoing electrons,

$$\varepsilon = E_0 - E_a - E_b, \tag{1}$$

$$\vec{q} = \vec{p}_0 - \vec{p}_a - \vec{p}_b. \tag{2}$$

Under high impact energy and high-momentum-transfer conditions, PWIA usually provides a good description of the $(e, 2e)$ reaction and the ionized electron essentially undergoes a clean "knockout" collision, as prescribed by the binary encounter approximation. The residual ion acts as a spectator in the $(e, 2e)$ reaction, and the target bound-electron momentum $\vec{p}$ is equal in magnitude but opposite in sign to the recoil ion momentum $\vec{q}$. The magnitude of the electron momentum p is related to the out-of-plane azimuthal angle ϕ between the two outgoing electrons,

$$p = \sqrt{\left(p_0 - \sqrt{2}p_a\right)^2 + 2p_a^2 \sin^2(\phi/2)}, \tag{3}$$

where p_0 and p_a ($p_a = p_b$) are the momenta of the incident electron and the outgoing electrons, respectively.

III. THEORETICAL CALCULATIONS

A full discussion of the theory of EMS and the various approximations made to calculate $(e, 2e)$ cross sections can be found in the literature [7–11]. Briefly, within the plane-wave impulse approximation (PWIA) framework, and the target Hartree-Fock approximation (THFA) or the target Kohn-Sham approximation (TKSA), the triple-differential cross section (TDCS) is given by

$$\frac{d^3\sigma}{d\Omega_a d\Omega_b dE_b} \propto S_i^f \int d\Omega |\psi_i(p)|^2, \tag{4}$$

where $\psi_i(p)$ is the momentum space representation of a canonical Hartree-Fock or Kohn-Sham orbital wave function, and S_i^f denotes the associated spectroscopic factor, which accounts for the shake-up processes due to configuration interactions in the final state. The atomic orbitals were calculated using the density functional theory (DFT) along with the standard hybrid Becke three-parameter Lee-Yang-Parr (B3LYP) functional method by means of the Amsterdam density functional (ADF) program. The nonrelativistic (NR) and the spin-orbital (SO) relativistic calculations were performed using the full-electron triple-zeta doubly polarized basis set (TZ2P) via the zero-order regular approximation (ZORA). The resulting atomic orbitals were used to generate the theoretical momentum space wave function. It is noted that the distortion interactions for all continuum electron wave functions are neglected in the present calculations.

The calculations have included the relativistic effects using the spin-orbit relativistic method. It is a two-component relativistic method which provides spin-orbit splitting components. The orbital wave function obtained has the following form [21],

$$\Psi(r) = \Psi_\alpha(r)\alpha + \Psi_\beta(r)\beta, \tag{5}$$

where α and β are the spin variables and which are orthogonal to each other. $\Psi_\alpha(r)$ and $\Psi_\beta(r)$ are the r space wave-function components for the spins α and β, respectively. The theoretical momentum profiles $|\Psi(p)|^2$ for the two-component orbitals are calculated through a Fourier transformation of the wave functions in r space as described in Eq. (6),

$$|\Psi(p)|^2 = |\Psi_\alpha(p)|^2 + |\Psi_\beta(p)|^2, \tag{6}$$

where $|\Psi_\alpha(p)|^2$ and $|\Psi_\beta(p)|^2$ are the momentum profiles of the spin α and β components.

IV. RESULTS AND DISCUSSIONS

An Hg atom has 80 electrons with a weight of about 200.59 atomic mass units. Its electronic configuration in the ground state can be written as $[\mathrm{Xe}]4f^{14}5d^{10}6s^2$.

Figure 1 presents the measured binding-energy spectrum of Hg obtained at an impact energy of about 1200 eV. It was constructed by summing all the genuine coincidence signals

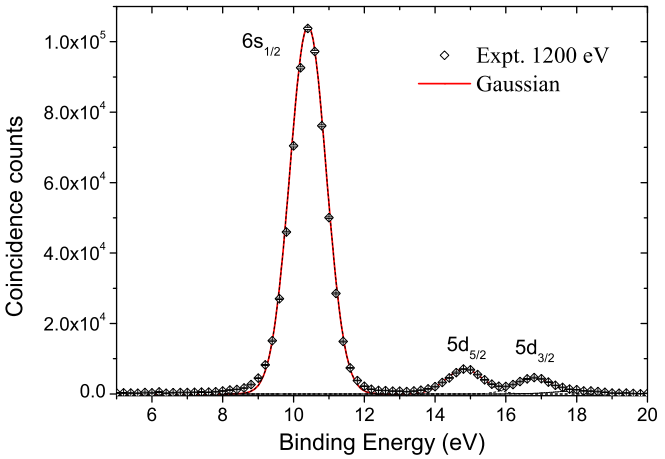

FIG. 1. Measured binding-energy spectrum summed over all azimuthal angles ϕ, obtained at an impact energy of about 1200 eV. The lines represent Gaussian fits to the data.

over the entire ϕ angles covered and by plotting the coincidence counts as a function of binding energy ε in the range from 5 to 20 eV. Three major peaks are clearly identified from the measured binding-energy spectrum in which a dominant peak can be seen at $\varepsilon = 10.4$ eV for the $6s_{1/2}$ orbital. It also shows a complete separation of the spin-orbit components of $5d_{5/2}$ and $5d_{3/2}$ orbitals at $\varepsilon = 14.9$ and 16.8 eV, respectively. To obtain the experimental momentum distribution for each orbital, the binding-energy spectra at the different ϕ angles were fitted with multiple Gaussian functions. The experimental momentum distributions were obtained by fitting the peak area for each orbital plotted as a function of the momentum p which was calculated from the azimuthal angle ϕ by Eq. (3).

The measured momentum distributions of the $6s_{1/2}$ orbital with impact energies of about 600 and 1200 eV are presented in Figs. 2(a) and 2(b) on linear and logarithmic scales, respectively. Also included in the figures are the nonrelativistic (NR) and the spin-orbital (SO) relativistic calculations under PWIA. The theoretical calculations have been folded with the instrumental momentum resolutions using a Monte Carlo method [37]. Here, the two theories differ strongly in magnitude, especially in the low-momentum region ($p < 0.5$ a.u.) where the calculated intensity by the NR is higher than the SO relativistic calculation. This phenomenon is consistent with earlier calculations by Mitroy and Fuss [12].

The experimental momentum distributions were measured on a relative scale, hence, to make a proper comparison between theories and experiment for the $6s_{1/2}$ orbital, we normalize the experimental momentum distributions to the SO relativistic calculation at the momentum origin ($p \sim 0$ a.u.). Here, the NR calculation has been renormalized by a factor of 0.73 to match the $p \sim 0$ height of the SO relativistic calculation [see the short dashed lines in Figs. 2(a) and 2(b)]. The experimental momentum distributions of the $6s_{1/2}$ orbital display a typical s-type characteristic with a maximum near the momentum origin. Such s-type momentum distributions are generally reproduced by both theories. Concerning the shape at low momenta ($p < 0.7$ a.u.), relatively good agreement is obtained between the experiment and the

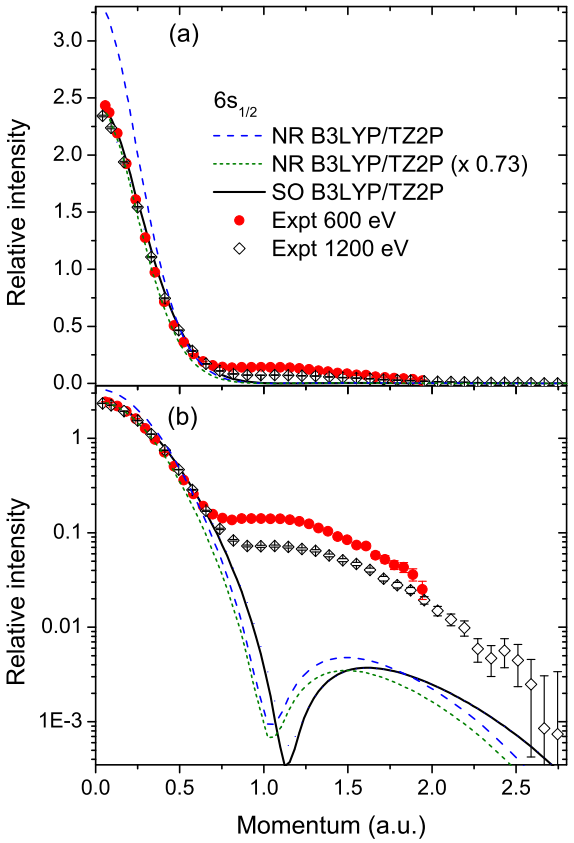

FIG. 2. Comparison of momentum profiles between experiment and theory for the $6s_{1/2}$ orbital of Hg in the linear plots of (a) and the logarithmic plots of (b). The solid circles and opened diamonds with error bars are the experimental data at impact energies of about 600 and 1200 eV, respectively. Solid lines: Spin-orbital (SO) relativistic calculation. Dashed lines: Nonrelativistic (NR) calculation. The short dashed curves are a renormalization of the NR calculation.

SO relativistic calculation. The nonrelativistic theory predicts a more sharply peaked momentum distribution. In general, a wave function in position space is uniquely related to the wave function in momentum space by a Fourier transformation. Here, the Fourier transform may affect largely the radial part of a wave function, namely, high density at small r leads to high density at large p and vice versa [7–11]. This means that the nonrelativistic theory will give a more diffuse orbital wave function for the $6s_{1/2}$ orbital of Hg than the SO relativistic theory.

In spite of the agreement in shape at low momenta between experiment and relativistic theory, however, one may notice some differences at high momenta for the $6s_{1/2}$ orbital. It would be easier to see the discrepancies in the logarithmic plots of Fig. 2(b) rather than the linear plots. The PWIA begins to deviate from the experiments at $p \sim 0.7$ a.u. In the high-momentum range ($p > 0.7$ a.u.) the experimental intensity is increased by roughly one order of magnitude compared with PWIA calculations, where the increased intensity is more evident at an impact energy of about 600 eV, and becomes smaller at 1200 eV. The PWIA calculations are unable to reproduce the higher intensity observed at high momenta for the $6s_{1/2}$ orbital.

The higher-momentum region of momentum profile involves contributions from the smaller r region, near the nucleus where potentials of the target atom and the residual ion may distort the electron waves from the plane waves. Such increased intensity in the high-momentum range can be qualitatively explained by the distortion of the incoming and outgoing electron waves in the target and the ion potentials since the size of the effect decreases with increasing impact energy [24]. Increased intensity at high momenta has been observed in the atomic ns orbitals of Ar, Kr, and Xe [38] where the distorted-wave calculations confirmed quantitatively the idea that the higher intensity in experiment at high momenta is associated with the distorted-wave effects. Other effects, such as electron correlation, have been mentioned in the literature as a possible reason for the higher intensity in experiment at high momenta [38].

The momentum distributions of the $5d$ orbitals of Hg are presented in Fig. 3. The individual one-electron-momentum distributions for the spin-orbit splitting components $5d_{5/2}$ and $5d_{3/2}$ were measured at impact energies of about 600 and 1200 eV, as shown in Figs. 3(a) and 3(b). The total $5d$ cross sections are presented in Fig. 3(c). Here, the theoretical momentum distributions have been carried out using the SO and NR calculations in which the $5d_{5/2}$ and $5d_{3/2}$ momentum distributions have been obtained individually by the SO relativistic theory, while the nonrelativistic theory gives the same shape and magnitude for both momentum distributions.

To compare the experimental momentum distributions with theories, a normalization procedure is needed because the measured $(e, 2e)$ momentum profiles are not on an absolute scale. A global normalization factor was determined by fitting the total $5d$ cross sections for 600- and 1200-eV impact energies to the theoretical one at $p \sim 1.4$ a.u. for both SO and NR calculations [13] [see in Fig. 3(c)], and then this factor was used to normalize the experimental one-electron-momentum profiles of the spin-orbit splitting components $5d_{5/2}$ and $5d_{3/2}$ in Figs. 3(a) and 3(b), respectively.

The theoretical momentum profiles yield a momentum density of zero at $p \sim 0$ a.u., and with a maximum at $p \sim 1.1$ a.u. for the SO calculations while the peak is located at $p \sim 1.23$ a.u. for the NR calculation. These calculations are generally consistent with the earlier EMS predictions on the $5d$ orbitals of Hg [12]. It is shown in the experimental momentum distributions that the peak intensity of the $5d_{5/2}$ orbital is higher than the $5d_{3/2}$ orbital. The figure shows that the SO calculations are in very good agreement with the experimental data in both the shape and the magnitude at high momenta ($p > 1.0$ a.u.), showing clearly that the SO relativistic wave functions are more realistic than the nonrelativistic ones. However, at low momenta ($p < 1.0$ a.u.), there is an unexpected higher intensity observed experimentally compared to both SO and NR calculations under PWIA, which has been called the turn-up effect in EMS [24]. Such turn-up effects can be qualitatively explained by the distortion of the incoming and outgoing electron waves in the target and the ion potentials, because the discrepancy between experiment and theory becomes smaller at an impact energy of 1200 eV in comparison with the results at 600 eV. The orbital symmetry analysis indicates that the low momenta can contribute to the electron density in the near nuclear region in atomic nd orbitals where distortion effects should be the strongest. Increased intensity at low momenta has been observed in the atomic nd orbitals of Xe, Cr, Zn, Mo, and Cd where the distorted-wave calculations confirmed that such distortion effects should decrease with increasing impact energy [24]. Unfortunately, theoretical calculations using the distorted-wave approximation for Hg have not been reported so far.

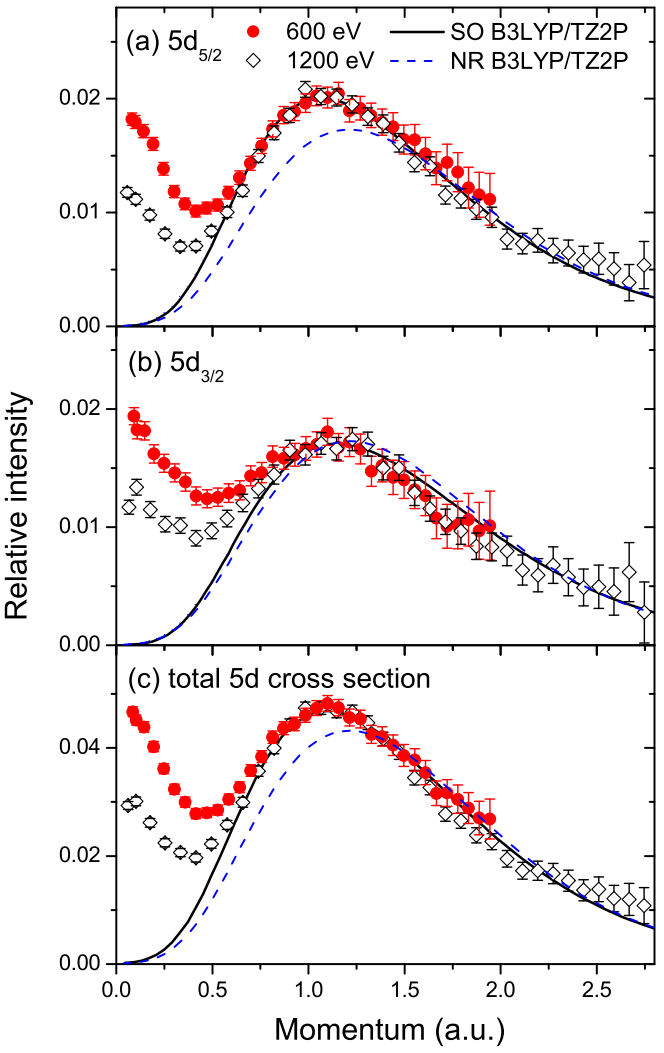

FIG. 3. Comparison of one-electron-momentum profiles between experiment and theory for $5d_{5/2}$ in (a), and $5d_{3/2}$ in (b); the total $5d$ cross sections are shown in (c). The solid circles and open diamonds with error bars are the experimental data at impact energies of about 600 and 1200 eV, respectively. Solid lines: Spin-orbital (SO) relativistic calculation. Dashed lines: Nonrelativistic (NR) calculation.

The branching ratio of $5d_{5/2} : 5d_{3/2}$ differential cross sections measured at an impact energy of 1200 eV is presented in Fig. 4 as a function of the momentum p. Nonrelativistic theory predicts that the branching ratio is independent on the momentum and is simply equal to the relative statistical weights, namely, 1.5:1, shown as the dashed curve in the figure, while the measured cross-section ratio deviates significantly from the constant value of 1.5, indicating directly the

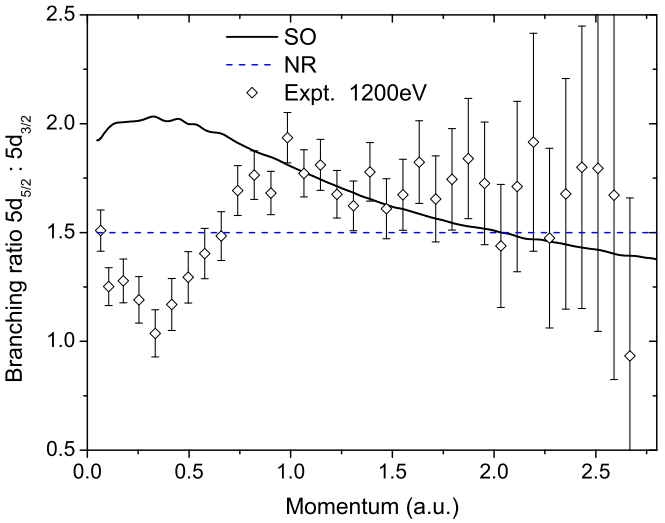

FIG. 4. The branching ratio of $5d_{5/2} : 5d_{3/2}$ cross sections as a function of the momentum for Hg. Solid lines: Spin-orbital (SO) relativistic calculation. Dashed lines: Nonrelativistic (NR) calculation. The open diamonds with error bars represent the experimental data at an impact energy of about 1200 eV.

influence of relativistic effects in the electronic structure of Hg. Also shown in the figure by the solid curve is the branching ratio given by the SO relativistic calculation. It agrees well with the experimental ratio in the high-momentum range ($p > 1.0$ a.u.). At low momenta ($p < 1.0$ a.u.) the relativistic SO calculation predicts a maximum located at $p \sim 0.3$ a.u. with a peak value of about 2 while a minimum is observed in the experimental data with a value of about 1. This is most likely due to the aforementioned distorted-wave effect which is not included in the present calculations.

V. CONCLUSIONS

We have reported a combined experimental and theoretical study of the electronic structure of the mercury (Hg) valence orbitals by electron-momentum spectroscopy (EMS). The electron-momentum profiles of the $6s$ and $5d$ orbitals were measured using a high-sensitivity binary $(e, 2e)$ spectrometer at impact energies of about 600 and 1200 eV. The binding-energy resolution of $\Delta\varepsilon \sim 1.1$ eV allows us to resolve clearly the spin-orbital splitting components $5d_{5/2}$ and $5d_{5/2}$ where the branching ratio of $5d_{5/2} : 5d_{3/2}$ as a function of the momentum shows directly the relativistic effect in the electronic structure of Hg.

The experimental momentum distributions for the individual orbitals were obtained and compared with the nonrelativistic (NR) and spin-orbital (SO) relativistic calculations within the plane-wave impulse approximation (PWIA). It was found that the SO calculations are in better agreement with the experimental data than the NR, showing clearly that the relativistic SO wave functions are more realistic than the nonrelativistic one. The current NR and SO relativistic calculations are generally consistent with the earlier EMS prediction of a relativistic effect in the valence orbitals of Hg [12], which has been justified by the present measurements.

At high momenta of $6s$ and low momenta of $5d$ orbital-momentum profiles, the experimentally observed intensity was higher than expected and also showed an energy dependence not predicted by the PWIA. These discrepancies can be qualitatively explained by the distortion of the incoming and outgoing electron waves in the target and the ion potentials since the discrepancy between experiment and theory decreases with increasing impact energy. Finally, it is to be noted that the present PWIA calculations are far from satisfactory for reproducing the higher intensity observed at high momenta of $6s_{1/2}$ and low momenta of $5d$ orbitals of Hg. More sophisticated models combining both distorted-wave approximation [23,38–40] and relativistic effects [41,42] are expected to fully describe the experimental $(e, 2e)$ momentum profiles of the valence orbitals of Hg.

ACKNOWLEDGMENTS

This work was supported by the National Natural Science Foundation of China under Grants No. 11774281, No. U1532263 and No. 11875219, Science Challenge Project No. TZ2016005. E.W. acknowledges support via a fellowship from the Alexander von Humboldt Foundation.

[1] B. A. Hess, *Relativistic Effects in Heavy-Element Chemistry and Physics* (Wiley, Hoboken, NJ, 2003).
[2] P. Pyykko, Chem. Rev. **88**, 563 (1988).
[3] P. Pyykko and J. P. Desclaux, Acc. Chem. Res. **12**, 276 (1979).
[4] S. Seidel and K. Seppelt, Science **290**, 117 (2000).
[5] M. W. Hussong, W. T. Hoffmeister, F. Rominger, and B. F. Straub, Angew. Chem. Int. Ed. **54**, 10331 (2015).
[6] F. Calvo, E. Pahl, M. Wormit, and P. Schwerdtfeger, Angew. Chem., Int. Ed. **52**, 7583 (2013).
[7] C. E. Brion, Int. J. Quantum Chem. **29**, 1397 (1986).
[8] I. E. McCarthy and E. Weigold, Rep. Prog. Phys. **54**, 789 (1991).
[9] M. A. Coplan, J. H. Moore, and J. P. Doering, Rev. Mod. Phys. **66**, 985 (1994).
[10] M. Vos and I. E. McCarthy, Rev. Mod. Phys. **67**, 713 (1995).
[11] M. Takahashi, Bull. Chem. Soc. Jpn. **82**, 751 (2009).
[12] J. Mitroy and I. Fuss, J. Phys. B **15**, L367 (1982).
[13] J. P. D. Cook, J. Mitroy, and E. Weigold, Phys. Rev. Lett. **52**, 1116 (1984).
[14] L. Frost, J. Mitroy, and E. Weigold, J. Phys. B **19**, 4063 (1986).
[15] S. Braidwood, M. Brunger, and E. Weigold, Phys. Rev. A **47**, 2927 (1993).
[16] X. G. Ren, C. G. Ning, J. K. Deng, G. L. Su, S. F. Zhang, and Y. R. Huang, Phys. Rev. A **73**, 042714 (2006).
[17] Z. Li, X. Chen, X. Shan, X. Xue, T. Liu, and K. Xu, Chem. Phys. Lett. **457**, 45 (2008).
[18] J. S. Zhu, J. K. Deng, and C. G. Ning, Phys. Rev. A **85**, 052714 (2012).

[19] K. Liu, C. G. Ning, and J. K. Deng, Phys. Rev. A **80**, 022716 (2009).
[20] K. Liu, C. Ning, Z. Luo, L. Shi, and J. Deng, Chem. Phys. Lett. **497**, 229 (2010).
[21] K. Liu, C.-G. Ning, and J.-K. Deng, Chin. Phys. Lett. **27**, 073403 (2010).
[22] J. P. D. Cook, I. E. McCarthy, J. Mitroy, and E. Weigold, Phys. Rev. A **33**, 211 (1986).
[23] M. Zhao, X. Shan, S. Niu, and X. Chen, Chin. Phys. B **26**, 093103 (2017).
[24] C. E. Brion, Y. Zheng, J. Rolke, J. J. Neville, I. E. McCarthy, and J. Wang, J. Phys. B **31**, L223 (1998).
[25] X. Ren, C. Ning, J. Deng, S. Zhang, G. Su, F. Huang, and G. Li, Chem. Phys. Lett. **404**, 279 (2005).
[26] C. G. Ning, X. G. Ren, J. K. Deng, G. L. Su, S. F. Zhang, and G. Q. Li, Phys. Rev. A **73**, 022704 (2006).
[27] X. Ren, C. Ning, J. Deng, S. Zhang, G. Su, Y. Huang, and G. Li, J. Electron Spectrosc. Relat. Phenom. **151**, 92 (2006).
[28] X. G. Ren, C. G. Ning, J. K. Deng, S. F. Zhang, G. L. Su, F. Huang, and G. Q. Li, Phys. Rev. Lett. **94**, 163201 (2005).
[29] M. J. Brunger, S. W. Braidwood, I. E. McCarthy, and E. Weigold, J. Phys. B **27**, L597 (1994).
[30] X. Wang, S. Xu, C. Ning, O. Al-Hagan, P. Hu, Y. Zhao, Z. Xu, J. Deng, E. Wang, X. Ren, A. Dorn, and D. Madison, Phys. Rev. A **97**, 062704 (2018).
[31] C. Lee, W. Yang, and R. G. Parr, Phys. Rev. B **37**, 785 (1988).
[32] A. D. Becke, J. Chem. Phys. **98**, 5648 (1993).
[33] X. G. Ren, C. G. Ning, J. K. Deng, S. F. Zhang, G. L. Su, F. Huang, and G. Q. Li, Rev. Sci. Instrum. **76**, 063103 (2005).
[34] X.-G. Ren, C.-G. Ning, J.-K. Deng, S.-F. Zhang, G.-L. Su, B. Li, and X.-J. Chen, Chin. Phys. Lett. **22**, 1382 (2005).
[35] C.-G. Ning, S.-F. Zhang, J.-K. Deng, K. Liu, Y.-R. Huang, and Z.-H. Luo, Chin. Phys. B **17**, 1729 (2008).
[36] C. G. Ning, J. K. Deng, G. L. Su, H. Zhou, and X. G. Ren, Rev. Sci. Instrum. **75**, 3062 (2004).
[37] P. Duffy, M. E. Cassida, C. Brion, and D. Chong, Chem. Phys. **159**, 347 (1992).
[38] Y. Miyake, M. Takahashi, N. Watanabe, Y. Khajuria, Y. Udagawa, Y. Sakai, and T. Mukoyama, Phys. Chem. Chem. Phys. **8**, 3022 (2006).
[39] X. Ren, S. Amami, O. Zatsarinny, T. Pflüger, M. Weyland, A. Dorn, D. Madison, and K. Bartschat, Phys. Rev. A **93**, 062704 (2016).
[40] D. H. Madison and O. Al-Hagan, J. At. Mol. Opt. Phys. **2010**, 367180 (2010).
[41] O. Zatsarinny and K. Bartschat, J. Phys. B **46**, 112001 (2013).
[42] C. J. Bostock, D. V. Fursa, and I. Bray, Phys. Rev. A **82**, 022713 (2010).